

Article

Anti-Explosion Performance of Composite Blast Wall with an Auxetic Re-Entrant Honeycomb Core for Offshore Platforms

Fang Luo, Shilian Zhang * and Deqing Yang

State Key Laboratory of Ocean Engineering, School of Naval Architecture, Ocean and Civil Engineering, Shanghai Jiao Tong University, 800 Dongchuan Road, Shanghai 200240, China; shaker900@163.com (F.L.); yangdq@sjtu.edu.cn (D.Y.)

* Correspondence: slzhang@sjtu.edu.cn; Tel.: +86-136-2190-3228

Received: 31 January 2020; Accepted: 5 March 2020; Published: 7 March 2020



Abstract: To improve the anti-explosion performance of blast wall in offshore platforms, an auxetic re-entrant blast wall (ARBW) was proposed and designed based on the indentation resistance effect of an auxetic structure. Based on the numerical nonlinear dynamic analysis method verified by the explosion experiment of a conventional steel corrugated blast wall (CBW), the failure mechanisms of ARBW, steel honeycomb sandwich blast wall (HSBW) and CBW were investigated under distributed impulse loads. Computational results demonstrated the excellent anti-explosion performance of the proposed ARBW design. Concerning the minimal deformation at the mid-point of the proposed protective structures, the ARBW performed best. As regards the minimal deformation at the connection, both ARBW and HSBW worked well. The stress distribution of the connection illustrated the different energy absorption and transmission modes of the three blast walls.

Keywords: blast wall; explosion; distributed impulse loads; auxetic; re-entrant honeycomb; corrugated plate; negative Poisson's ratio; offshore platform

1. The State-of-the-Art Blast Wall Design in Offshore Platforms

Studies on impulse destruction are an important part of marine engineering protective design. Different protective structures lead to disparate anti-explosion performances under the same impulse loading. At the present time, a popular form of protective structures is corrugated blast wall (CBW), which has been applied to offshore platforms due to its considerable blast-resistant performance and easy availability. A usual design of the CBW in offshore platforms is shown in Figure 1 [1]. Because of the number of explosion accidents on offshore platforms in recent years [2], higher defense requirements have been put forward regarding the impact resistance of the blast wall. Although the analysis method in the design guidance of protective structures has developed from single degree of freedom (SDOF) to nonlinear finite element analysis (NLFEA) [3–5], the typical design scheme in the guidance is a blast wall made by a corrugated plate.

Several methods have been used to strengthen the capability of blast resistance. J.W.Boh et al. [6] presented a passive impact barrier system placed at a certain offset behind the walls. Nwankwo E. et al. [7] presented the development of a rapid assessment tool which provided an understanding of the effect of a composite patch on the blast resistance of profiled blast walls. Christian W. et al. [8] carried out an investigation into the influence of inclined angle of a Vee stiffener used on a blast wall structure. The results showed that the alteration of the inclined angle had a considerable effect on the dynamic response of the blast wall structure. These methods offer a certain reinforcement to the CBW, but the reinforcement is somewhat limited. New shapes of blast wall with high anti-explosion performance need to be studied.

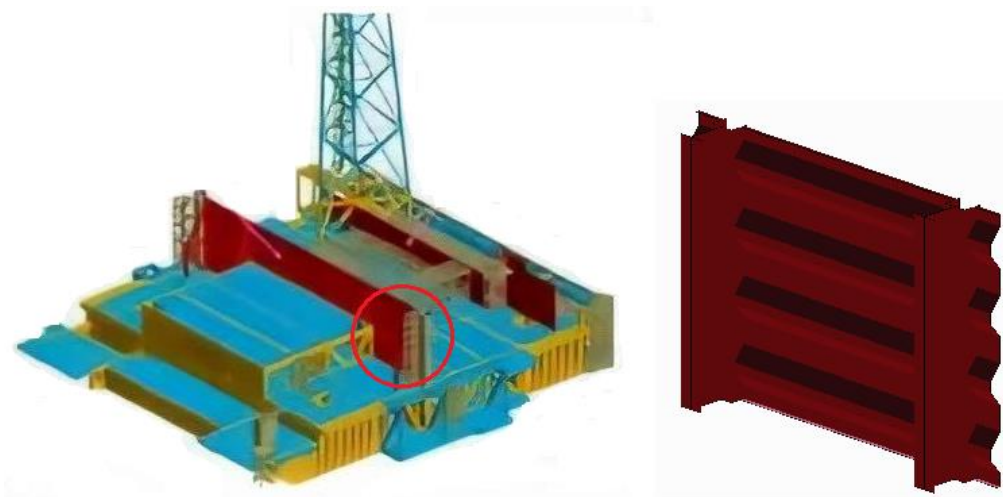


Figure 1. A usual design of the corrugated blast wall (CBW) in offshore platforms.

Honeycomb sandwich plates are another choice for the anti-blast structure. Some research works have shown that sandwich structures possess anti-blast behavior [9]. M.D. Theobald et al. [10] conducted air-blast tests on sandwich panels composed of steel face sheets with unbonded aluminum foam or hexagonal honeycomb cores. The results showed that face sheet thickness has a significant effect on the performance of the panels relative to an equivalent monolithic plate. Zhu F et al. [11] simulated the blast impact of square metallic sandwich panels and compared them with the results of experimental investigation. Pydah A. et al. [12] analyzed transient elasto-plastic deformations of two-core sandwich plates with and without a bumper and subjected them to blast loads with the objective of ascertaining the energy dissipated due to plastic deformations.

Auxetic re-entrant structures are different from traditional sandwich structures. They shrink laterally during compression and expand laterally during stretching, which provides better fracture toughness, shear modulus, energy absorption and anti-fatigue crack growth [13,14]. Junhua Zhang et al. [15] discussed in detail the case of nonlinear transient response and showed that honeycomb sandwich plates with a negative Poisson's ratio perform better than those with a positive Poisson's ratio. Deqing Yang et al. [16] compared the explosion resistance of honeycomb structures with different negative Poisson's ratios and layer number arrangements, which simulated the penetration and failure mode of the structure under underwater explosion shock. Chang Qi et al. [17] investigated experimentally and numerically the responses of auxetic honeycomb-cored sandwich panels as protective systems under impact. Gabriele Imbalzano et al. [18] compared the different fragmentation forms of negative Poisson's ratio honeycomb structures and traditional honeycomb structures under a localized explosion. Hohammad M.H. [19] reinforced the facesheets of auxetic honeycomb plates by carbon nanotubes (CNTs) considering agglomeration effects. At present, there is insufficient research into the honeycomb structure with an auxetic effect under impulse loading. Further applications are needed regarding the design of explosion-proof structures for offshore platforms.

This paper proposes a new design of ARBW, and also a HSBW design for comparison for offshore platforms. The deformation, stress and strain distribution of the ARBW and HSBW under distributed impulse loading are numerically investigated. For the purpose of verification, the responses of the CBW with the same outer dimensions and mass are obtained. The failure mechanism of three kinds of blast wall are revealed. The computational results showed that both the ARBW and HSBW have excellent energy absorption performance.

2. Schematic Design of ARBW, HSBW and CBW

2.1. Design of CBW

The CBW design is based on a non-symmetric trapezoidal deep trough profile, with angle connections at the top and bottom and free sides. The corrugated part is 880 mm wide, 915 mm long and 40.5 mm deep. The whole part is 2 mm thick. The connection is 195 mm deep and 35 mm long. It is composed of 3 mm and 4 mm stainless-steel angles welded to a 12 mm thick angle that forms the primary framework. The mass of the blast plate, made of stainless steel, is 41.5 kg. The model shown in Figure 2 is consistent with the test scheme [20]. For the test results, the 10.27 KPa·s distributed impulse is selected for the simulation, which caused a 22.2 mm permanent deformation of the mid-point [21].

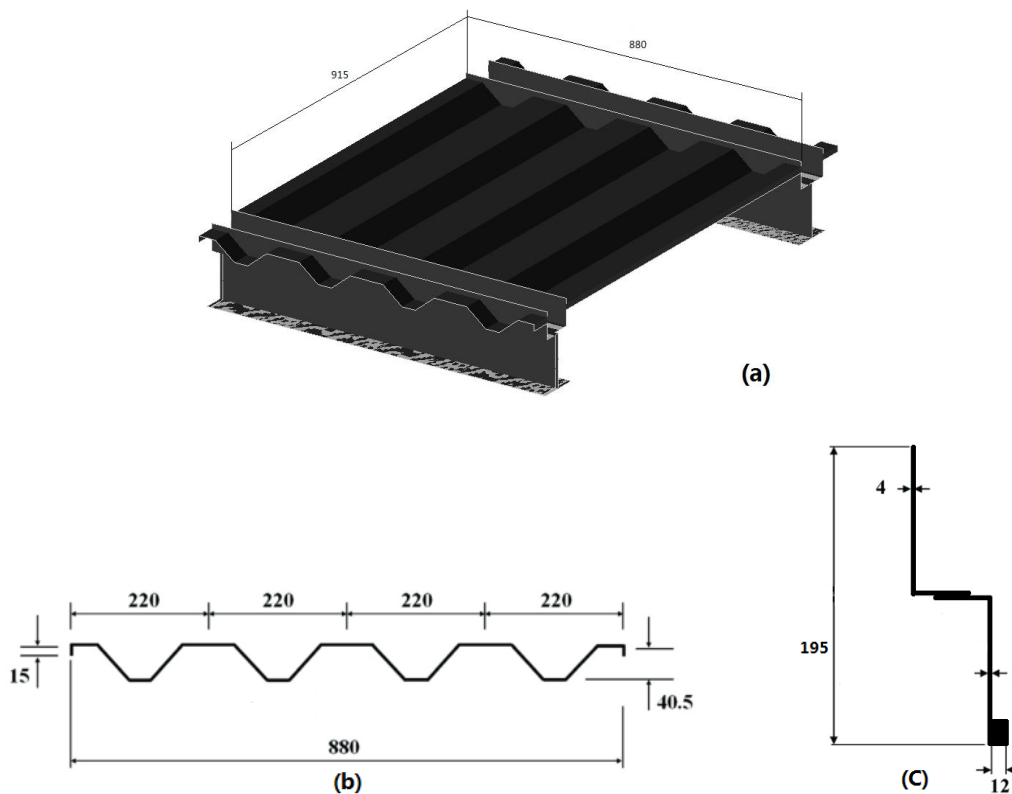


Figure 2. CBW (a) model (b) dimensions of corrugated panel (c) dimensions of connection.

2.2. Design Descriptions of ARBW and HSBW

The ARBW is composed of the auxetic unit cell with a re-entrant shape. According to [16], when the cell angle is 60° and there are layers, the auxetic honeycomb structure presents the smallest plastic deformation. Therefore, the topological cell is selected as a single-cell configuration. The horizontal length h is 52.15 mm, the inclined length l is 26.31 mm, the cell wall thickness is 2.2 mm, and the cell angle θ is 60° . The cell configuration and design of the ARBW are shown in Figure 3. The thickness of the upper and lower faceplates is 0.1 mm, respectively. The negative Poisson's rate is calculated as -3.87 [16]. The relative density $\rho^*_{auxetic}$ is 4.74%, which is obtained by dividing the area occupied by the structure and the total area.

The HSBW is composed by the conventional honeycomb unit cell with a typical cellular structure. The cell angle is 120 degrees, the height h is 27 mm, the inclined length l is 15.59 mm, and the cell wall thickness is also 2.2 mm. The cell configuration and design of the HSBW re shown in Figure 4. The thickness of the upper and lower faceplates is 0.1 mm, respectively. The relative density $\rho^*_{honeycomb}$ is 2.67%, which is obtained by dividing the area occupied by the structure and the total area.

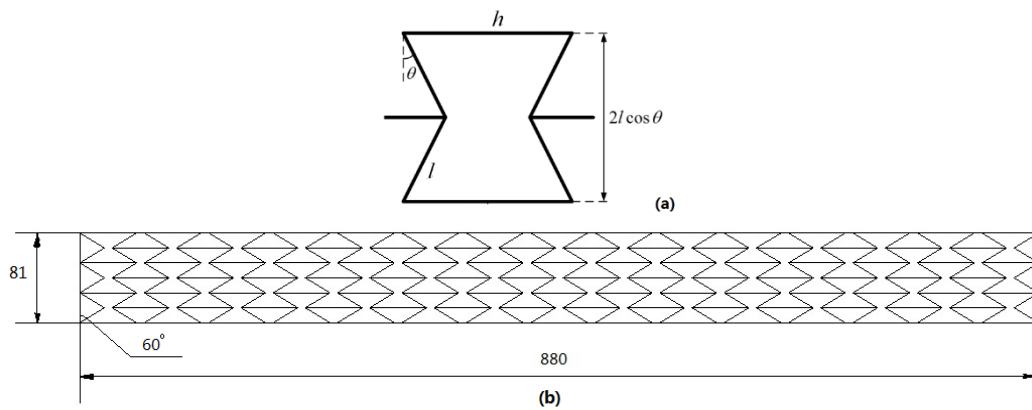


Figure 3. Cell configuration and design of the auxetic re-entrant blast wall (ARBW). (a) auxetic unit cell, (b) auxetic layout.

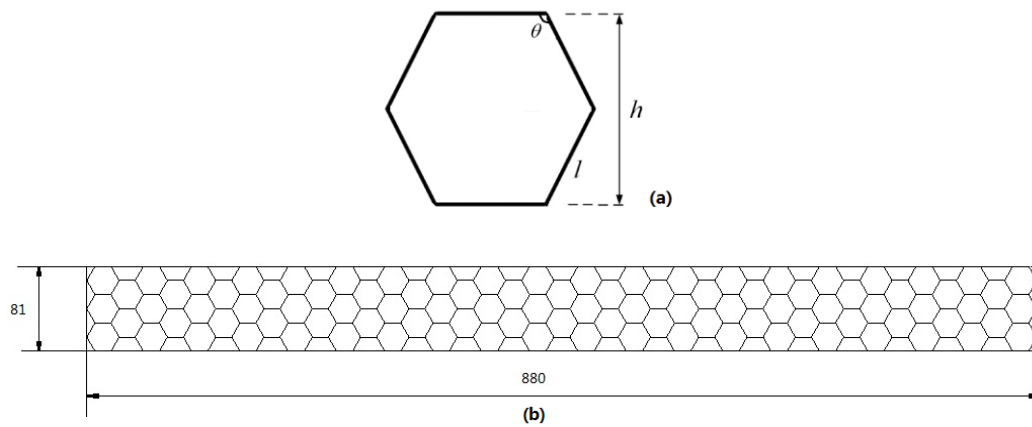


Figure 4. Cell configuration and design of the honeycomb sandwich blast wall (HSBW). (a) honeycomb unit cell, (b) honeycomb layout.

2.3. Model Diagrams of ARBW and HSBW

The model diagrams of the ARBW and HSBW are presented in Figure 5. These structures are both used to form a three-layer composite blast wall. The length, width, and height are 915 mm, 880 mm, and 81 mm, respectively. The thickness of the upper and lower faceplates is 0.1 mm. The overall mass is under 41.5 kg using stainless steel. Both models are entirely fixed to the framework made by the connection. The connection of the two models is the same as the connection of the CBW model.

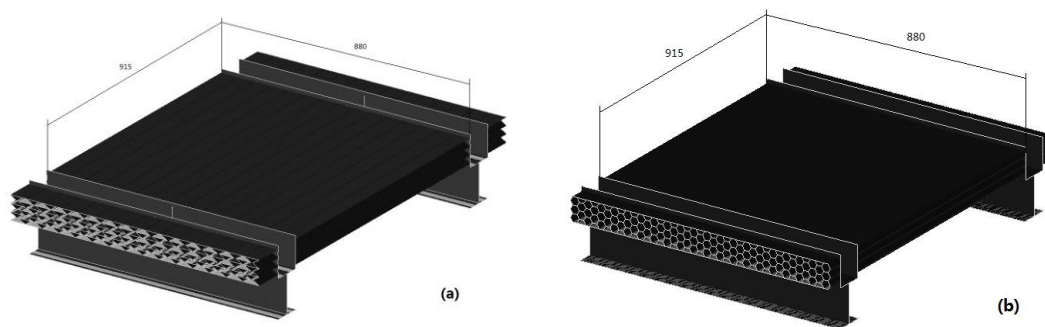


Figure 5. Model diagrams: (a) ARBW, (b) HSBW.

3. Numerical Models of Anti-Explosion Analysis for the Proposed Blast Wall

3.1. Material Model

Stainless steel is used in the experimental CBW model. The Cowper–Symonds yielding model, as shown in Equation (1), is suitable for describing the properties of stainless-steel structures if the thermal deformation effect is negligible. This model accurately describes the large deformation of the material and the high strain change.

$$\frac{\sigma_y}{\sigma_0} = 1 + \left(\frac{\dot{\epsilon}}{D}\right)^{\frac{1}{q}} \tag{1}$$

where σ_0 is the static yield strength, $\dot{\epsilon}$ is an equivalent plastic strain, and D and q are material constants. The parameters of the steel are presented in Table 1 [21].

Table 1. Material parameters of stainless steel.

E (GPa)	ν	P (Kg/m ³)	σ_0 (MPa)	$\dot{\epsilon}$	D	q
210	0.3	7850	276	17.76%	2720	5.78

3.2. Finite Element Model

Finite element models of the three kinds of blast wall are shown in Figure 6. All are simulated by plate elements, and all elements are defined by pshell. The element numbers of ARBW, HSBW and CBW are 74,648, 88,730 and 20,252, respectively. Point 1 is the mid-point of the whole panel and point 2 is the junction between the panel and connection. These evaluation points are used to measure the anti-explosion performance after the calculation is finished.

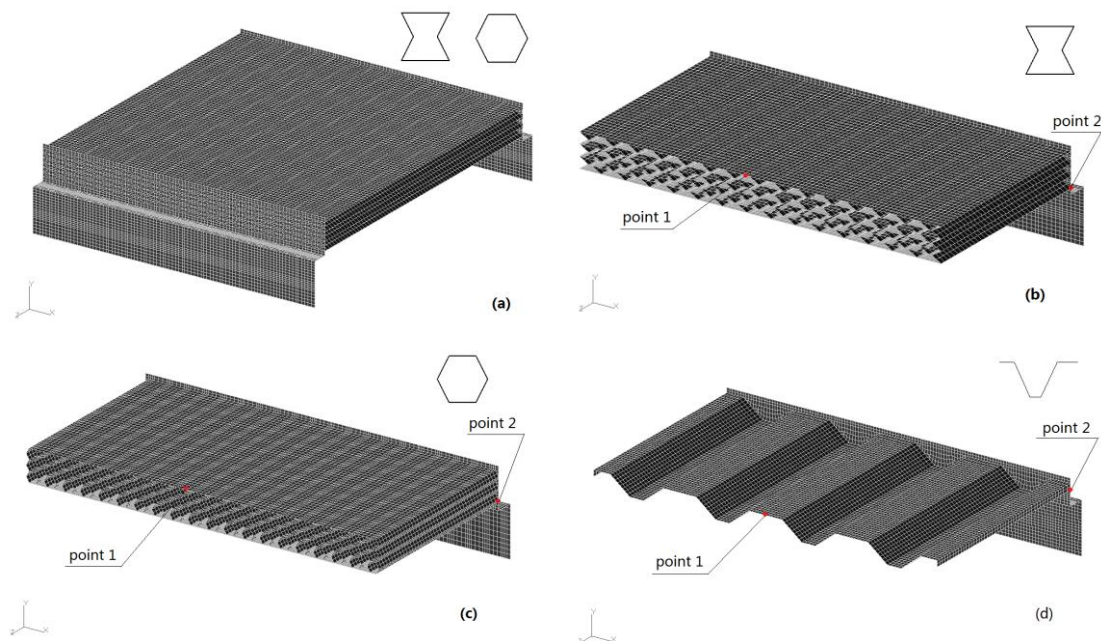


Figure 6. Finite element models: (a) the whole model, (b) 1/2 symmetry of the ARBW, (c) 1/2 symmetry of Table 1. symmetry of the CBW.

3.3. Loadings and Constraints

The bottom of each model is fixed. The distributed impulse loading is applied to the faceplate along the y-direction. The distributed impulse loading is a triangular shock wave, with a peak value of 123 KPa. The applied time is 0.167 seconds, so the unit impulse is 10.27 KPa·s. The distributed impulse loading and constraints are shown in Figure 7.

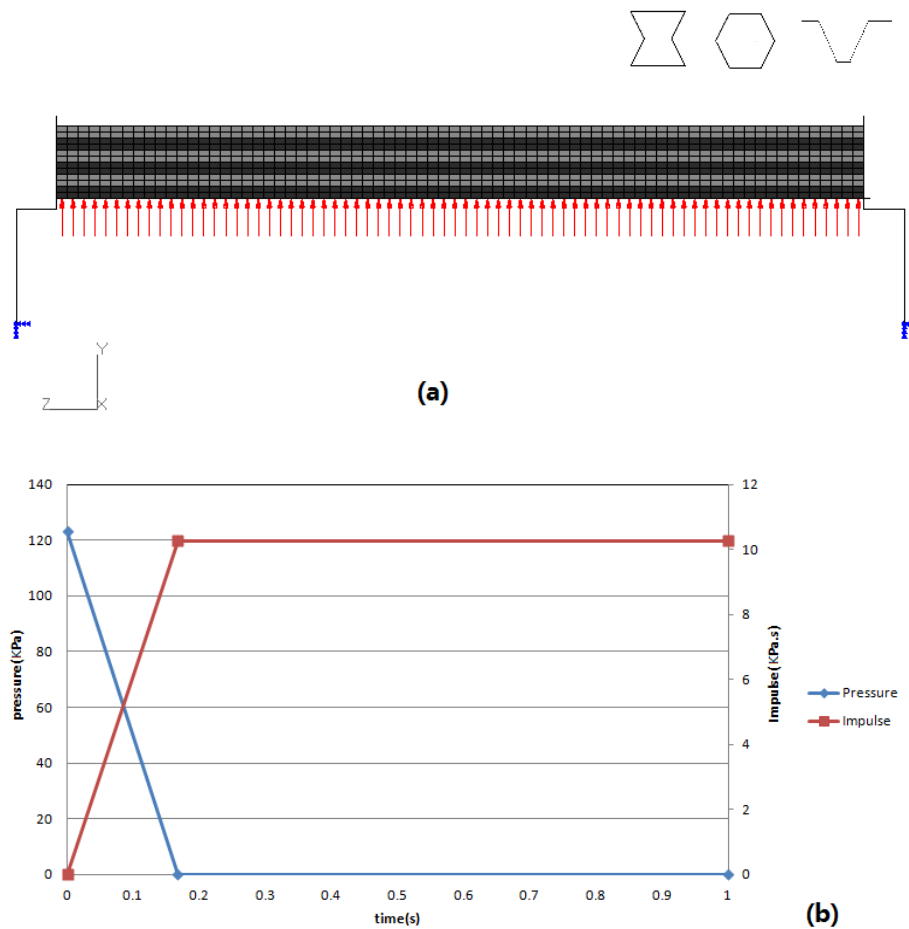


Figure 7. Distributed impulse loading and constraints. (a) The distributed impulse loading and constraints. (b) The pressure and impulse applied on the models.

4. Comparative Analysis of Anti-Explosion Performance

The computational results of the ARBW and HSBW under distributed impulse loading are compared with the CBW results. Deformation, stress and strain are selected to measure the anti-explosion performance.

4.1. Deformation

The deformation of the ARBW is shown in Figure 8. The bottom faceplate was deformed plastically. The maximum deformation occurred at the free side. The upper faceplate showed a small bulging from the beginning of the test until it reached stability. The auxetic core was crushed, reducing the transmitted pressure. The connection was vertically stretched.

The deformation of the HSBW is shown in Figure 9. Evidently, the honeycomb panel did not present any core densification effect. The whole sandwich panel worked as a bending beam. The upper and bottom faceplates showed the same deformation behavior. No maximum deformation and cell collapse occur at the free side. The connection was stretched vertically and horizontally.

The deformation of the CBW is presented in Figure 10. The whole panel is bent at the beginning of the test. The middle part recovered, but the free side buckled permanently by the end of the test. Evidently, the maximum deformation occurred at the free side. The connection was stretched vertically and horizontally.

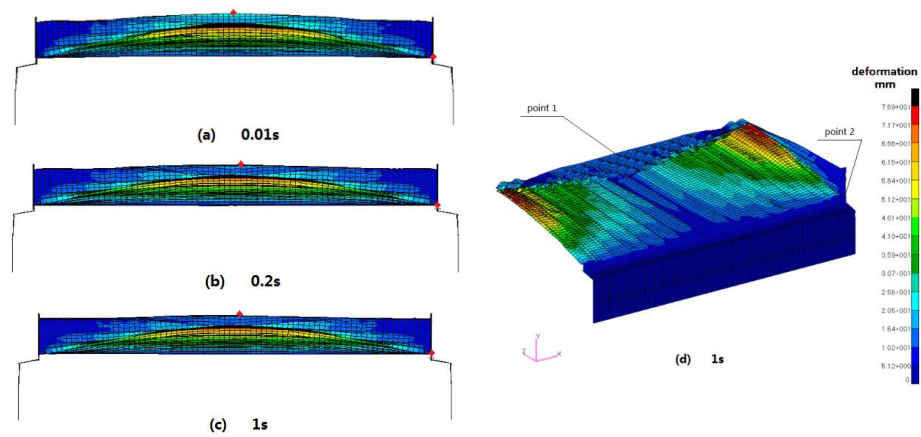


Figure 8. Deformation of the ARBW. (a) the moment of 0.01 s, (b) the moment of 0.2 s, (c) the moment of 1 s, (d) the moment of 1 s in isometric view.

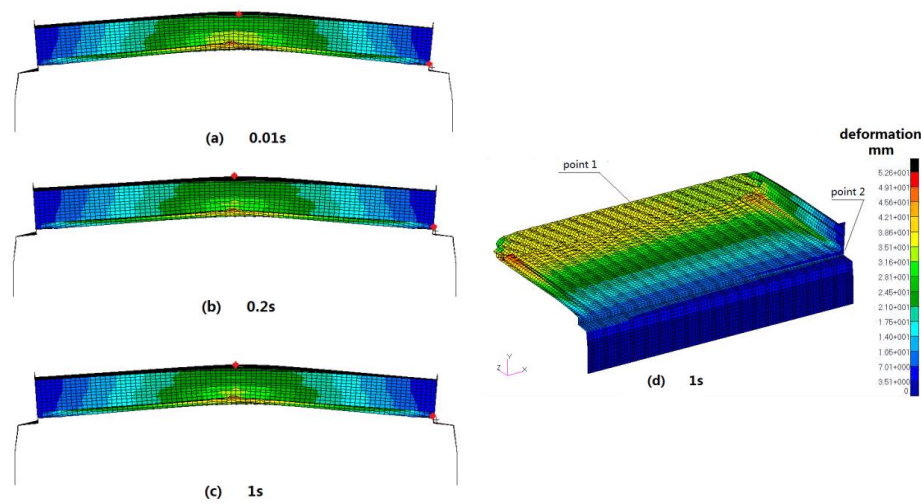


Figure 9. Deformation of the HSBW. (a) the moment of 0.01 s, (b) the moment of 0.2 s, (c) the moment of 1 s, (d) the moment of 1 s in isometric view.

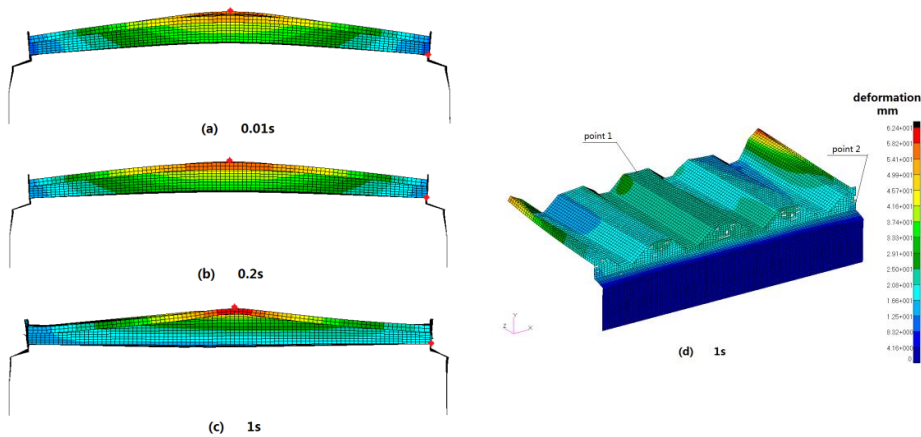


Figure 10. Deformation of the CBW. (a) the moment of 0.01 s, (b) the moment of 0.2 s, (c) the moment of 1 s, (d) the moment of 1 s in isometric view.

4.2. Resistance Performance Evaluation

The deformation histories of the evaluation points on the blast walls are shown in Figure 11. Point 1 presents the deformation of the whole blast wall. It can be seen that the peak deformation occurred at the beginning of the test, and the peak value of ARBW was less than the others. The permanent deformation appeared at the end. The permanent value of CBW was 23 mm, which corresponds with the test result mentioned in Section 2.1. The permanent value of ARBW was still the lowest. Both the values of ARBW and HSNW were stable during the shock. Point 2 shows the deformation of the connection. The permanent values of ARBW and HSBW were under 8 mm.

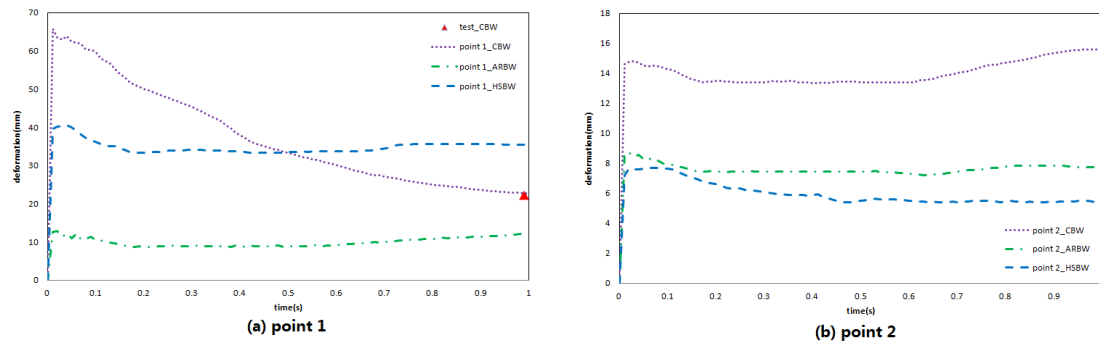


Figure 11. Deformation history of the evaluation points of blast walls: (a) point 1, (b) point 2.

The deformation difference history shown in Figure 12 is between point 1 and point 2. This is used to measure the energy absorption through large deformation. Obviously, the deformation differences of HSBW and CBW corresponded with the deformations of point 2. The energy absorption of ARBW could hardly be evaluated by the deformation difference, but this could be demonstrated by the stress diagram.

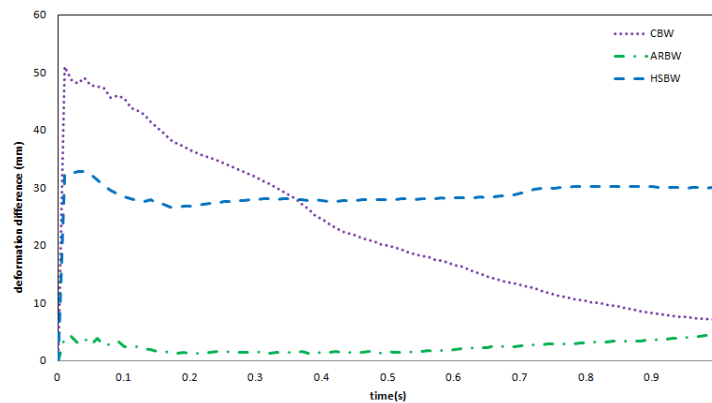


Figure 12. Deformation difference history of blast walls.

4.3. Stress Distribution

The stress distribution of the ARBW is shown in Figure 13. The cells close to the facesheet collapsed immediately at the beginning of the test and redistributed the shock. The neighboring cells were drawn to the center of the panel due to the auxetic behavior. After stress redistribution, the entire ARBW was uniformly damaged, extending from the panel to the connection. The stress distribution of the connection was almost homogeneous except for the 12 mm angle after shock.

The stress distribution of the HSBW is shown in Figure 14. Evidently, the honeycomb panel absorbed the shock energy through bending. The stress of the connection was lower than the stress of the honeycomb panel during the explosion. The maximum stress occurred at cells which were near the free sides.

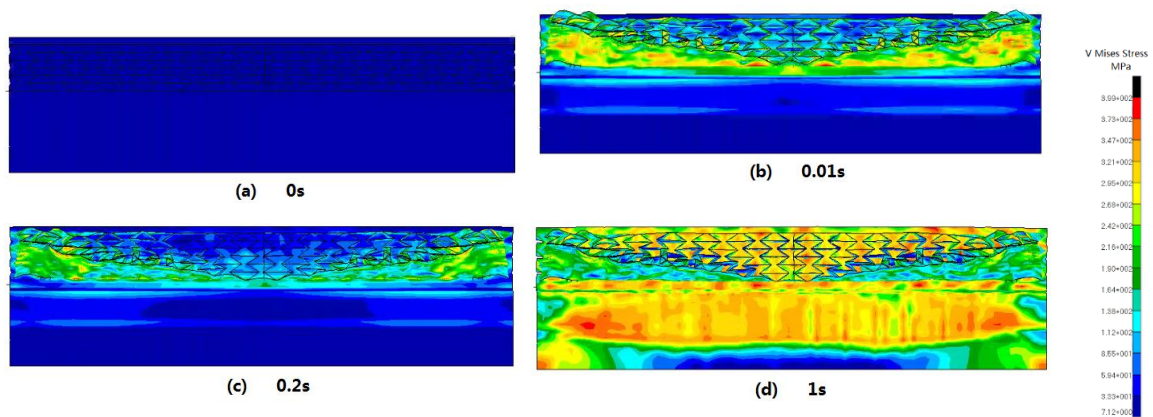


Figure 13. Stress distribution of the ARBW under impulse loads. (a) the moment of 0 s, (b) the moment of 0.01 s, (c) the moment of 0.2 s, (d) the moment of 1 s.

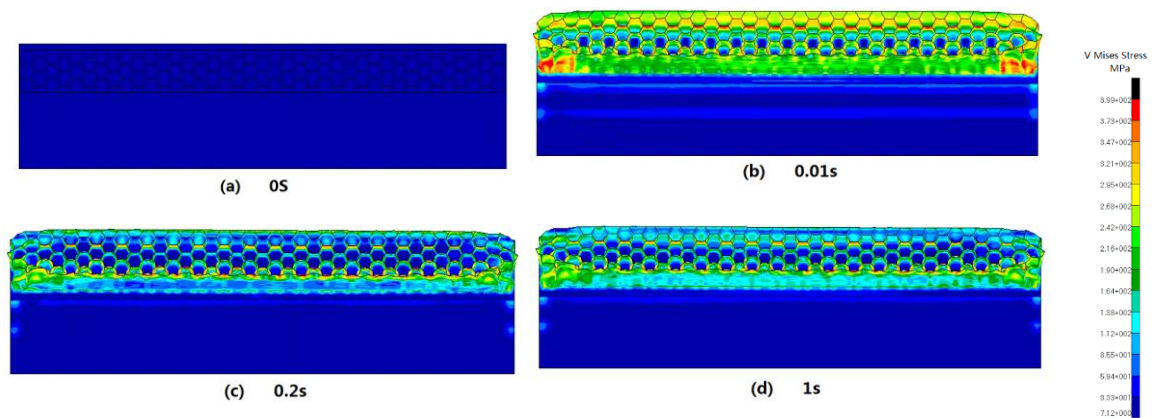


Figure 14. Stress distribution of the HSBW under impulse loads. (a) the moment of 0 s, (b) the moment of 0.01 s, (c) the moment of 0.2 s, (d) the moment of 1 s.

The stress distribution of the CBW is shown in Figure 15. The maximum stress occurred on the connection at the beginning of the explosion. After the panel recovered, the stress was transmitted to the connection non-uniformly. The disappearance of some elements showed that a localized failure occurred on the 4 mm angle near the panel. The strain distribution was able to explain the element failure better.

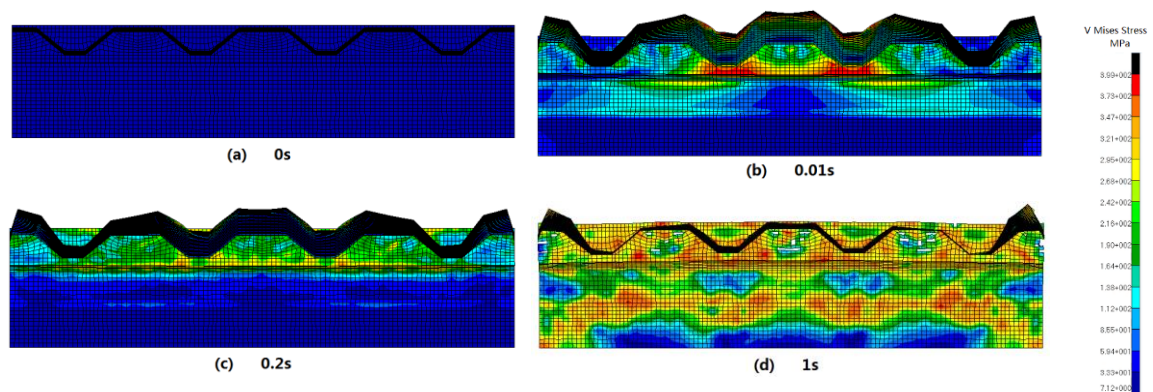


Figure 15. Stress distribution of the CBW under impulse loads. (a) the moment of 0 s, (b) the moment of 0.01 s, (c) the moment of 0.2 s, (d) the moment of 1 s.

4.4. Failure Mechanism

The permanent strain distribution of the blast wall is shown in Figure 16. The maximum plastic strain of ARBW and HSBW was under 17.76%. Although the cells at the panel edge collapsed, the most plastic strain of ARBW happened at the panel corner, which shows that the cell-collapsed edge was strengthened due to the densification effect. Besides the panel corner, most of the plastic strain of HSBW occurred symmetrically at the panel center. The maximum plastic strain of CBW happened at the connection, at 17.76%. The connection could not withstand the shock energy and partially failed at the 4 mm angle near the panel, although the 3 mm flexible angle yielded at first.

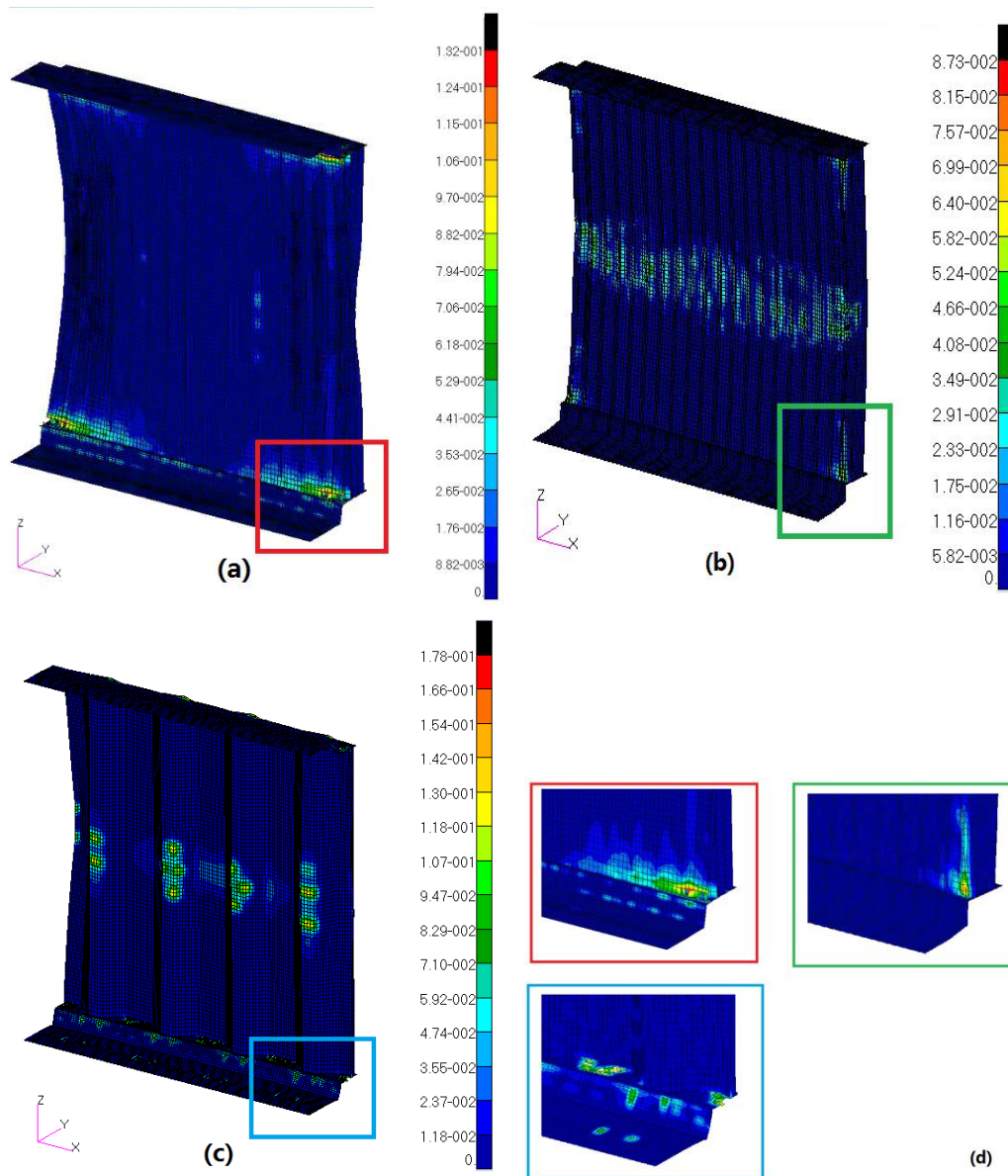


Figure 16. Permanent strain distribution of the blast walls: (a) ARBW; (b) HSBW; (c) CBW; (d) corner of blast wall.

5. Conclusions

Numerical investigations of the dynamic responses and energy-absorbing properties of ARBW, HSBW and CBW under distributed impulse loading were conducted. Comparison with experimental

results revealed different protective mechanisms of the three kinds of blast walls. This study provided support for the protective structure design of offshore platforms. Key observations are as follows:

- For the ARBW and the HSBW, the distributed impulse loading was absorbed through panel deformation. The ARBW works with crushable cells with auxetic behavior, which the HSBW achieves through whole panel bending.
- To measure the anti-explosion performance, the deformation difference can be used for the HSBW and the CBW, but this hardly works for the ARBW. The stress diagram of the ARBW can demonstrate energy absorption and redistribution because of the auxetic mechanism.
- As regards the deformation of point 2, both the ARBW and the HSBW protected the connection well. With regard to the stress of the connection, the HSBW performed better. Concerning point 1, the ARBW provided the best anti-explosion performance.
- The cell-collapsed edge of ARBW was strengthened due to the densification effect. The plastic failure of CBW happened at the connection first, which meant that the connection absorbed shock energy and partially failed.

Author Contributions: Model analysis and writing—original draft preparation, F.L.; writing—review and editing, D.Y. and S.Z.; All authors have agreed in both contents and form of the final version, being F.L. the responsible of this article. All authors have read and agreed to the published version of the manuscript.

Funding: This research was funded by the National Natural Science Foundation of China (51479115) and Opening Project by the State Key Laboratory of Ocean Engineering (GKZD010071).

Conflicts of Interest: The authors declare no conflict of interest.

References

1. Syed, Z.I.; Mohamed, O.A.; Rahman, S.A. Non-linear Finite Element Analysis of Offshore Stainless Steel Blast Wall under High Impulsive Pressure Loads. *Procedia Eng.* **2016**, *145*, 1275–1282. [[CrossRef](#)]
2. Summerhayes, C. Deep Water—The Gulf Oil Disaster and the Future of Offshore Drilling. *Underw. Technol.* **2011**, *30*, 113–115. [[CrossRef](#)]
3. Brewerton, R. *Design Guide for Stainless Steel Blast Wall, Technical Note 5*; Fire and Blast Information Group: London, UK, 1999.
4. Walker, S.; Bleach, R.; Carney, S.; Fairlie, G.; Louca, L.A. New guidance on the design of offshore structures to resist the explosion hazard. In Proceedings of the OMAE03, Cancun, Mexico, 8–13 June 2003.
5. Paik, J. Design of offshore facilities to resist gas explosion hazard, engineering handbook. *Ships Offshore Struct.* **2006**, *1*, 165–169. [[CrossRef](#)]
6. Boh, J.W.; Louca, L.A.; Choo, Y.S. Energy absorbing passive impact barrier for profiled blastwalls. *Int. J. Impact Eng.* **2005**, *31*, 976–995. [[CrossRef](#)]
7. Nwankwo, E.; Fallah, A.S.; Langdon, G.S.; Louca, L.A. Inelastic deformation and failure of partially strengthened profiled blast walls. *Eng. Struct.* **2013**, *46*, 671–686. [[CrossRef](#)]
8. Christian, W.; Kim, B.T. Behaviors of a Blast Wall According to the Angle of Vee Stiffener. *Appl. Mech. Mater.* **2012**, *152*, 856–859.
9. Dharmasena, K.P.; Wadley, H.N.G.; Xue, Z.; Hutchinson, J.W. Mechanical response of metallic honeycomb sandwich panel structures to high-intensity dynamic loading. *Int. J. Impact Eng.* **2008**, *35*, 1063–1074. [[CrossRef](#)]
10. Theobald, M.D.; Langdon, G.S.; Nurick, G.N.; Pillay, S.; Heyns, A.; Merrett, R.P. Large inelastic response of unbonded metallic foam and honeycomb core sandwich panels to blast loading. *Compos. Struct.* **2010**, *92*, 2465–2475. [[CrossRef](#)]
11. Zhu, F.; Zhao, L.M.; Lu, G.X. A numerical simulation of the blast impact of square metallic sandwich panels. *Int. J. Impact Eng.* **2009**, *36*, 687–699. [[CrossRef](#)]
12. Pydah, A.; Batra, R.C. Blast loading of bumper shielded hybrid two-core Miura-ori/honeycomb core sandwich plates. *Thin Walled Struct.* **2018**, *129*, 45–57. [[CrossRef](#)]
13. Zhang, X.W.; Yang, D.Q. Mechanical Properties of Auxetic Cellular Material Consisting of Re-Entrant Hexagonal Honeycombs. *Materials* **2016**, *9*, 900. [[CrossRef](#)] [[PubMed](#)]

14. Bezazi, A.; Scarpa, F. Mechanical behaviour of conventional and negative Poisson's ratio thermoplastic polyurethane foams under compressive cyclic loading. *Int. J. Fatigue* **2007**, *29*, 922–930. [[CrossRef](#)]
15. Zhang, J.H.; Zhu, X.F.; Yang, X.D.; Zhang, W. Transient nonlinear responses of an auxetic honeycomb sandwich plate under impact loads. *Int. J. Impact Eng.* **2019**. [[CrossRef](#)]
16. Yang, D.Q.; Zhang, X.W.; Wu, B.H. The Influence Factors of Explosion and Shock Resistance Performance of Auxetic Sandwich Defensive Structures. *J. Shanghai Jiaotong Univ.* **2018**, *52*, 379–387.
17. Qi, C.; Remennikov, A.; Pei, L.Z.; Yang, S.; Yu, Z.H.; Ngo, T.D. Impact and close-in blast response of auxetic honeycomb-cored sandwich panels: Experimental tests and numerical simulations. *Compos. Struct.* **2017**, *180*, 161–178. [[CrossRef](#)]
18. Imbalzano, G.; Linforth, S.; Ngo, T.D.; Lee, P.V.S.; Tran, P. Blast resistance of auxetic and honeycomb sandwich panels: Comparisons and parametric designs. *Compos. Struct.* **2018**, *183*, 242–261. [[CrossRef](#)]
19. Hajmohammad, M.H.; Kolahchi, R.; Zarei, M.S.; Nouri, A.H. Dynamic response of auxetic honeycomb plates integrated with agglomerated cnt-reinforced face sheets subjected to blast load based on visco-sinusoidal theory. *Int. J. Mech. Sci.* **2019**. [[CrossRef](#)]
20. Langdon, G.S.; Schleyer, G.K. Inelastic deformation and failure of profiled stainless steel blast wall panels. part ii: Analytical modelling considerations. *Int. J. Impact Eng.* **2005**, *31*, 371–399. [[CrossRef](#)]
21. Schleyer, G.; Langdon, G. *Pulse Pressure Testing of 1/4 Scale Blast Wall Panels with Connections*; HSE Research Report: Sudbury, UK, 2003.



© 2020 by the authors. Licensee MDPI, Basel, Switzerland. This article is an open access article distributed under the terms and conditions of the Creative Commons Attribution (CC BY) license (<http://creativecommons.org/licenses/by/4.0/>).